Absorbing boundary conditions for water wave simulation in the vicinity of a solid body

Jose M. Orellana

Comptes Rendus
Mécanique
Draft

Absorbing boundary conditions for water wave simulation in the vicinity of a solid body

José Marie Orellana[a]

[a] Laboratoire de modélisation mathématique et numérique (M2N), Conservatoire des Arts et Métiers, 292, rue Saint Martin 75141 PARIS Cedex 03 France

E-mail: jose.orellana@lecnam.net (J.M. Orellana)

Abstract. In this paper, we focus on the modelling of the wake of a solid body moving through a body of water. To this end, the flow of an inviscid, barotropic and compressible fluid around the solid body regarded as motionless is examined. The dynamic behavior of the fluid is analyzed by means of a two-dimensional Neumann-Kelvin's coupled model enhanced with capillarity and inertia terms. For computational purposes, the unbounded spatial domain has to be truncated by artificial boundaries. Difficulties arise when it comes to setting appropriate absorbing boundary conditions for a waves propagation problem in a stratified convective fluid media with significant differences between layer properties. Numerical illustrations of the results are given and commented.

Keywords. Absorbing boundary conditions, fluid-structure interaction, water waves propagation, numerical simulations.

2020 Mathematics Subject Classification. 76N99.

This article is a draft (not yet accepted!)

Version française abrégée

Afin de déterminer le sillage d'un corps en mouvement dans une étendue d'eau, on considère l'écoulement d'un fluide non visqueux, barotrope et compressible autour de celui-ci. On étudie la propagation d'une petite perturbation dans ce milieu considéré comme un fluide stratifié en mouvement quasi uniforme à l'aide d'un modèle couplé de type Neumann-Kelvin tenant compte de la capillarité et de l'inertie de la surface du fluide. Pour réaliser la simulation numérique, il est nécessaire de délimiter artificiellement le domaine et d'introduire des conditions aux limites absorbantes adaptées. Les résultats obtenus sont analysés et commentés.

1. Introduction

Understanding wave propagation mechanisms on a body of water has long been an interesting topic for many researchers [1–6]. Surface water wave phenomenon is due to the balance between the gravity forces that keep horizontal free surface of the water, the surface tension that keeps the consistency of the air-water interface, the water inertia and the difference between air and water pressures. According to the relevant effect that forces the motion, the waves are usually divided in gravity waves, capillary waves or pressure waves. In this work, the surface waves of interest are generated by the movement of a solid body, propagate all around it and interact with its rigid surface leading to a wake in its vicinity [7–9]. Unlike common approaches where the water body is viewed as a homogeneous propagating medium [2–6], here it is considered as a stratified structure made of two infinite liquid layers with very different properties [1, 10, 11]. The upper layer is the free surface water with an infinitesimal thickness and small characteristic velocity of wave propagation namely, riddle velocity. The lower layer is the inner water with a finite or semi infinite thickness and with a high characteristic velocity of wave propagation namely the speed of sound in water. In addition to better encompass the properties of the propagating waves, a two dimensional Neumann-Kelvin's coupled model enhanced with capillarity and inertia terms is proposed [12–14]. The classic method for handling such a problem consists in considering the whole unbounded structure and then introducing a radiation boundary conditions at infinity when analytic treatment is feasible or in truncating the given domain and then applying High Order Absorbing Boundary Conditions [15–17] or Perfectly Matched Layer method [18–20] on the boundaries artificially chosen to solve it numerically [21, 22]. The main concern is that non-reflecting boundary condition should accurately represents the solution in the infinite domain outside for the arbitrarily bounded domain [23] and ideally, the solutions calculated in both cases should be identical. Nevertheless to avoid increasing the amount of calculations and the number of auxiliary variables involved, an approximate low order absorbing boundary condition is first sought.

After stating the problem and specifying underlying assumptions, a linearization around a steady state is performed and different accurate boundary conditions are introduced to carry out the study. The variational formulation of the problem is deduced and a finite element approximation in space with a centered finite difference scheme in time are used to approach the solution. Results obtained are illustrated and discussed.

2. Problem statement

Our purpose is to determine the dynamical behavior of the water surface in the vicinity of a solid body that moves with an horizontal velocity U and with a possible oscillatory displacement. To this end, we examine the irrotationnal and inviscid flow of a compressible and barotropic fluid around the structure seen as fixed. Due to the existence of singularities at contact points between solid body surface and the surface of water, and also at underwater angular points [24], the structure is immersed and its shape is simplified to a cylinder. We consider as computational domain a rectangular open domain Ω with a hole of radius R in its center. Its boundary $\partial\Omega = \Gamma_0 \cup \Gamma_1 \cup \Gamma_s \cup \Gamma_2 \cup \Gamma_b$ has unit outward normal vector ν. Γ_0 corresponds to the bottom of the system, Γ_s, to the free surface of the water, Γ_1 and Γ_2, to the sides through which the water flow enters and leaves Ω and Γ_b , to the rigid body surface (see figure 1). $\partial\Gamma_s$ denotes the edges of Γ_s. A steady flow passes through Ω with horizontal velocity U and a small disturbance is introduced in the fluid as an initial condition.

3. Theoretical modelling

In most cases, a common formulation of this wave propagation problem consists in finding for a fluid medium regarded as homogeneous, the velocity potential Φ satisfying the Laplace's equation and the vertical displacement of the surface η verifying [1, 2] :

- The kinematic boundary conditions

$$\frac{\partial \Phi}{\partial \nu} = U.\nu \text{ on } \Gamma_0 \cup \Gamma_b \times]0, T[, \tag{1}$$

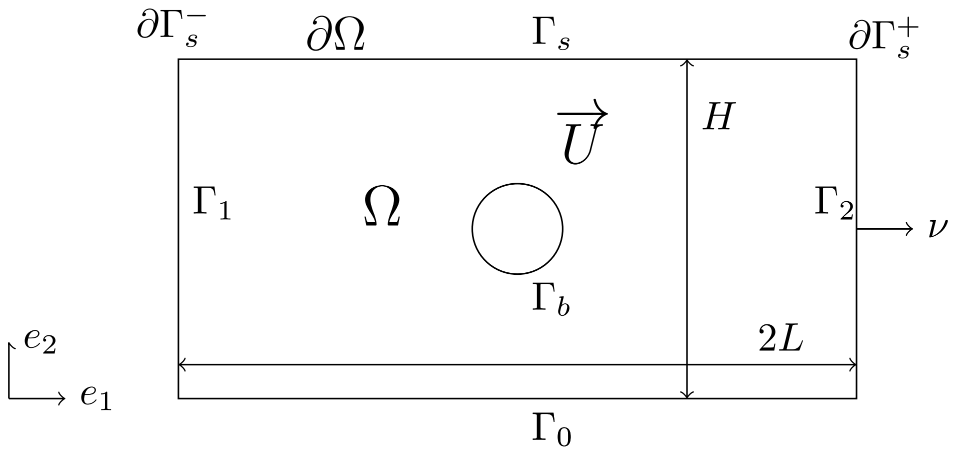

Figure 1. Geometry and notations of the problem.

$$\frac{\partial\Phi}{\partial\nu} = \frac{\partial\eta}{\partial t} + \nabla_s\Phi\cdot\nabla_s\eta \quad \text{on} \quad \Gamma_s\times]0,T[. \tag{2}$$

- The dynamic boundary conditions

$$\frac{\partial\Phi}{\partial t} - \frac{1}{2}||\nabla_s\Phi||^2 - g\eta = 0 \quad \text{on} \quad \Gamma_s\times]0,T[. \tag{3}$$

- The radiation boundary conditions based on the behavior of the solution in the neighborhood of infinity

$$\nabla\Phi \to 0 \text{ as } |x_1| \to \infty,\ t\in]0,T[. \tag{4}$$

Incompressibility of the flow is assumed since the water for flow speeds much smaller than the sound speeds in the water. Capillarity and inertia of the fluid surface are also neglected. In the following, as the propagating medium is regarded as a bounded stratified compressible fluid waveguide with a convective uniform mean flow, the Laplace's continuity equation, the dynamic boundary conditions Eq.(3) and the radiation boundary conditions Eq.(4) have to be modified.

3.1. *Hypotheses and formulation of the global model*

The propagating medium considered consists of two liquid layers with very different properties and then two differnt models have to be introduced to take these features into account : an inner fluid model and a surface model.

3.1.1. *Formulation of the inner fluid model*

We assume that the flow is characterized by two variables modelling the mass density ρ_{tot} and the velocity potential Φ that satisfy :

- The conservation of mass equation

$$\frac{\partial\rho_{tot}}{\partial t} + div(\rho_{tot}\nabla\Phi) = 0 \text{ in } \Omega\times]0,T[. \tag{5}$$

- The Bernoulli equation for unsteady compressible potential flow (neglecting gravity effect)

$$\frac{\partial\Phi}{\partial t} + \frac{1}{2}||\nabla\Phi||^2 + F(\rho_{tot}) = 0 \text{ in } \Omega\times]0,T[\tag{6}$$

where $F(\rho_{tot}) = \int_{\rho_0}^{\rho_{tot}} \frac{1}{\rho}.\frac{\partial p}{\partial \rho} d\rho + F(\rho_0)$ is the barotropic potential, p, the fluid pressure and T, the simulation time.

3.1.2. *Formulation of the surface model*

Applying Newton's second law of motion to an infinitesimal small surface element of thickness 2ε that vertically moves of a displacement η_{tot}, leads to the free surface equilibrium equation :

$$2\varepsilon\rho_{tot}\frac{D^2\eta_{tot}}{Dt^2} = -\rho_{tot}\frac{\partial\Phi}{\partial t} - \frac{\rho_{tot}}{2}||\nabla_s\Phi||^2 + \sigma\Delta_s\eta_{tot} - \rho_{tot}g\eta_{tot} \quad \text{in} \quad \Gamma_s\times]0,T[\tag{7}$$

where the forces involved consist in the capillary action $\sigma\Delta_s\eta_{tot}$ with σ the surface tension, the gravity force $-\rho_{tot}g\eta_{tot}$ and the pressure $-\rho_{tot}\partial\Phi/\partial t - \rho_{tot}||\nabla_s\Phi||^2/2$. From a mathematical point of view, capillary term stabilizes the partial differential equation [14]. The subscript s indicates that the differential operator is considered locally along a surface namely here Γ_s.

3.1.3. *On the interface*

The kinematic boundary condition Eq.(2) becomes the continuity of normal velocity at the interface :

$$\frac{\partial\eta_{tot}}{\partial t} + \nabla_s\Phi\cdot\nabla_s\eta_{tot} = \frac{\partial\Phi}{\partial\nu} \quad \text{in} \quad \Gamma_s\times]0,T[\tag{8}$$

taking account of the rotation of the normal to the surface.

3.2. *Linearization of the governing equations*

The global nonlinear dynamical model obtained is linearized around a main steady state. Therefore the global solution is split into the steady state obtained and a transient one. The lateral boundary conditions are defined separately according to the nature of the state. For the steady flow, the most realistic condition is to fix the normal velocity. For transient flow, non-reflecting boundary conditions have to be prescribed for the inlet and the outlet of Ω in order to avoid any spurious reflections of the waves reaching the boundaries of the domain.

3.2.1. *Main background steady state flow*

We introduce φ_0, the velocity potential corresponding to a steady quasi uniform horizontal steady flow of an incompressible fluid which enters and leaves Ω at constant unit horizontal velocity with normal surface displacement variation along Γ_s regarded as negligible and non penetrability condition on $\Gamma_0\cup\Gamma_b$ satisfied. This background flow is stationary with respect to the boat which is chosen as frame of reference. φ_0 is the solution to the following problem :

$$\begin{cases} -\Delta\varphi_0 = 0 \;\text{ in } \Omega \text{ and } \displaystyle\int_{\Gamma_s}\varphi_0 = 0, \\[2ex] \dfrac{\partial\varphi_0}{\partial\nu} = 0 \;\text{ on } \Gamma_0\cup\Gamma_b\cup\Gamma_s, \\[2ex] \dfrac{\partial\varphi_0}{\partial\nu} = (e_1\cdot\nu) \text{ in } \Gamma_1\cup\Gamma_2. \end{cases} \tag{9}$$

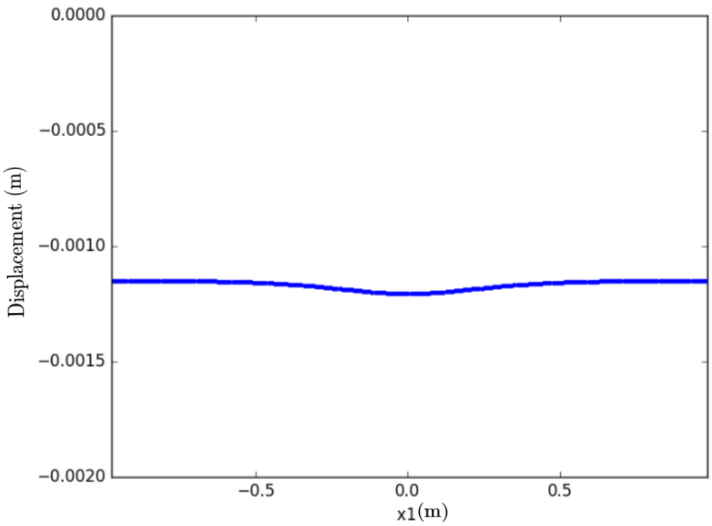

Figure 2. Free surface vertical displacement η_0 (m) solution of Eq.(10) versus x_1 (m) with the 'digging' effect.

To obtain the related displacement on the surface η_0 of this flow for our model, stationary balance of forces on free surface Eq.(7) along with homogeneous Neumann boundary conditions are applied. According to the frame of reference, it leads in stationary case to :

$$\begin{cases} 2\varepsilon\rho_0 U^2 \nabla_s\varphi_0\cdot\nabla_s\left(\nabla_s\varphi_0\cdot\nabla_s\eta_0\right)+\sigma\Delta_s\eta_0-\rho_0 g\eta_0=-\dfrac{\rho_0}{2}U^2\|\nabla_s\varphi_0\|^2 \quad \text{in} \quad \Gamma_s, \\ \dfrac{\partial\eta_0}{\partial\nu_s}=0 \quad \text{on} \quad \partial\Gamma_s \end{cases} \tag{10}$$

with ρ_0, the fluid density and g, the gravity acceleration. The solution of Eq.(9) corresponds to a steady quasi uniform horizontal flow with a digging effect due to the term $-\rho_0 U^2\|\nabla_s\varphi_0\|^2/2$ as shown in figure 2. The order of magnitude of free surface strain is about $10^{-3}m$ and therefore negligible in comparison with initial computational domain Ω dimensions.

3.2.2. *Transient state*

We study the evolution of a small disturbance around the steady state $(\rho_0,\varphi_0,\eta_0)$. The unsteady waves in the fluid are represented by the perturbation functions ρ,φ,η of variables $x(x_1,x_2)$ and t. The problem is formulated with them wherein $\rho_{tot}(x,t)=\rho_0(x)+\rho(x,t)$, $\Phi(x,t)=U\varphi_0(x)+\varphi(x,t)$, $\eta_{tot}(x,t)=\eta_0(x)+\eta(x,t)$. The solution is split into main background steady state component and a transient one. The domain Ω is then cropped by Γ_0, Γ_b, $\Gamma_s=\eta_0$, Γ_{1equi} and Γ_{2equi} as shown in figure 3. The new lateral boundaries Γ_{1equi} and Γ_{2equi} correspond to equipotential lines of φ_0 passing respectively through left upper domain corner and right upper corner of Ω. As result, the main steady flow crosses perpendiculary Γ_{1equi} and Γ_{2equi} and no tangential flow remains in the new domain Ω. The artificial boundaries are chosen far enough from rigid body to consider that steady state flow is uniform in this area and so the corners of the new domain are right-angled. The disturbance is so small that it is then reasonable to neglect the non-linear terms in the governing equations Eq.(5)-Eq.(8) to obtain Eq.(11)-Eq.(14). Convective derivatives with flow velocity $U\nabla\varphi_0$ are used to derive linearized equations Eq.(12) and Eq.(13). Hence (ρ,φ,η) are assured to satisfy the linearized enhanced Neumann-Kelvin's model with capillarity :

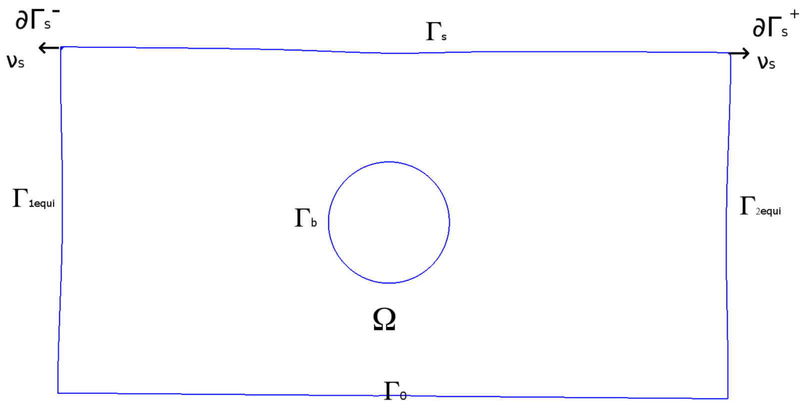

Figure 3. Calculated geometry of the new computational domain in the case of a solid body size large compared to initial computational domain. The digging effect on Γ_s and the inwards bowing of Γ_{1equi} and Γ_{2equi} are more pronounced than in our case.

- The linearized continuity equation

$$\frac{\partial \rho}{\partial t} + U\nabla\rho \cdot \nabla\varphi_0 + \rho_0 \Delta\varphi = 0 \quad \text{in} \quad \Omega \times]0,T[. \tag{11}$$

- The linearized momentum equation for the inner fluid

$$\frac{\partial^2 \varphi}{\partial t^2} + 2U\nabla\varphi_0 \cdot \nabla\left(\frac{\partial\varphi}{\partial t}\right) + U^2\nabla\varphi_0 \cdot \nabla(\nabla\varphi_0.\nabla\varphi) - c_f^2\Delta\varphi = 0 \text{ in } \Omega\times]0,T[\tag{12}$$

given that $\frac{1}{2}|\nabla\varphi_0|^2 + \nabla F(\rho_0) = 0$ and $\frac{\partial F(\rho_0)}{\partial \rho_{tot}} = \frac{c_f^2}{\rho_0}$.

- The linearized momentum equation for the surface fluid

$$2\varepsilon\rho_0\left(\frac{\partial^2\eta}{\partial t^2} + 2U\nabla_s\varphi_0 \cdot \nabla_s\left(\frac{\partial\eta}{\partial t}\right) + U^2\nabla_s\varphi_0 \cdot \nabla_s\left(\nabla_s\varphi_0 \cdot \nabla_s\eta\right)\right)$$
$$= \sigma\Delta_s\eta - \rho_0 g\eta - \rho_0\frac{\partial\varphi}{\partial t} - \rho_0 U\nabla_s\varphi_0 \cdot \nabla_s\varphi \quad \text{in} \quad \Gamma_s\times]0,T[\tag{13}$$

where $\cdot$ denotes the scalar product. Since the domain of study was reshaped, $\nabla_s\eta_0$ and $\Delta_s\eta_0$ are set to zero on Γ_s.

- The continuity of normal velocity at the interface

$$\frac{\partial\varphi}{\partial\nu} = \frac{\partial\eta}{\partial t} + U\nabla_s\varphi_0 \cdot \nabla_s\eta \quad \text{in} \quad \Gamma_s\times]0,T[. \tag{14}$$

- The non-penetrability condition leads to homogeneous Neumann boundary condition for φ

$$\frac{\partial\varphi}{\partial\nu} = 0 \quad \text{in} \quad \Gamma_0 \cup \Gamma_b \times]0,T[. \tag{15}$$

- The initial condition corresponding to a disturbance taking place in the fluid: the functions $\varphi(x,0)$ and $\partial\varphi/\partial t(x,0)$ are set as Gaussian pulse functions in Ω and the functions $\eta(x,0)$ and $\partial\eta/\partial t(x,0)$ are fixed to zero on Γ_s.

3.2.3. *Lateral artificial boundary conditions*

Non-reflecting boundary condition applied on inner fluid lateral edges is :

$$a\frac{\partial\varphi}{\partial t}+\left(U\frac{\partial\varphi_0}{\partial\nu}+c_f\right)\frac{\partial\varphi}{\partial\nu}=0 \quad \text{in} \quad \Gamma_{1equi}\cup\Gamma_{2equi}\times]0,T[\tag{16}$$

where c_f denotes the speed of sound in the fluid and a a parameter related to the angle of incidence waves with respect to the normal of the boundary surface. This relation is consistent with Sommerfeld-like non reflecting boundary condition for a wave which propagates at the phase velocity c_f corrected by the normal to the boundary of velocity component of the main background steady flow $U\partial\varphi_0/\partial\nu$. In the following the parameter a is set to 1, this implies that the angles of incidence of impinging disturbances are close to the normal of the boundary. For such an order of approximation of absorbing boundary condition, it is not beneficial to set $a\neq 1$ [17].

On the surface bounds $\partial\Gamma_s$ non-reflecting conditions imposed is the natural Sommerfeld-like non reflecting boundary condition,

$$\frac{\partial\eta}{\partial t}+\left(U\frac{\partial\varphi_0}{\partial\nu_s}+c_r\right)\frac{\partial\eta}{\partial\nu_s}=0 \quad \text{in} \quad \partial\Gamma_s \quad \forall t\in]0,T[\tag{17}$$

where c_r denotes the riddle velocity with $c_r^2=\sigma/2\rho_0\varepsilon$. It is consistent with the one dimensional non-reflecting boundary condition for a propagating wave at velocity c_r in an uniform background steady flow of velocity $U\partial\varphi_0/\partial\nu_s$. This boundary condition introduces a mathematical specific damping on each boundary nodes of the surface Γ_s in order to attenuate spurious reflecting modes.

4. Solution method

The classical approach for addressing waves propagation in layered media with a wave source close to interfaces by looking for a solution as a superposition of plane waves is not considered in the following [1, 10, 11]. Instead, a weak form of the problem and a finite element formulation are employed.

4.1. *Variational formulation and numerical approach*

Multiplying Eq.(12) by $\psi\in H^1(\Omega)$ and Eq.(13) by $\upsilon\in H^1(\Gamma_s)$ respectively together with Green's formula application lead to the following coupled variational formulation :

Find functions $(\varphi,\eta)\in H^1(\Omega)\times H^1(\Gamma_s)\times L^2(]0,T[)$ such that $\forall(\psi,\upsilon)\in H^1(\Omega)\times H^1(\Gamma_s)$

$$\begin{aligned}&\int_\Omega\ddot\varphi\psi\,d\tau+U\int_\Omega\nabla\varphi_0\cdot\left(\nabla\dot\varphi\psi-\dot\varphi\nabla\psi\right)d\tau+c_f\int_\Gamma\dot\varphi\psi\,d\tau+c_f^2\int_\Omega\nabla\varphi\cdot\nabla\psi\,d\tau\\&-U^2c_f^2\int_\Omega\left(\nabla\varphi_0\cdot\nabla\varphi\right)\left(\nabla\varphi_0.\nabla\psi\right)d\tau-c_f^2\int_{\Gamma_s}\dot\eta\psi\,d\tau-Uc_f^2\int_{\Gamma_s}\nabla_s\varphi_0\cdot\nabla_s\eta\,\psi\,d\tau=0\end{aligned} \tag{18}$$

and

$$\begin{aligned}
&2\varepsilon {c_f}^2 \int_{\Gamma_s} \left(\ddot{\eta} v + U \nabla_s \varphi_0 \left(\nabla_s \dot{\eta} v - \dot{\eta} \nabla_s v\right) - U^2 (\nabla_s \varphi_0 \cdot \nabla_s \eta)(\nabla_s \varphi_0 \cdot \nabla_s v)\right) d\sigma \\
&-2\varepsilon {c_f}^2 U \int_{\Gamma_s} \left(U v \Delta_s \varphi_0 \left(\nabla_s \varphi_0 \cdot \nabla_s \eta\right) + v \Delta_s \varphi_0 \dot{\eta}\right) d\sigma + \frac{c_f^2}{\rho_0} \int_{\Gamma_s} \sigma \nabla_s \eta . \nabla_s v \, d\sigma \\
&+ \frac{c_f^2}{\rho_0} \int_{\Gamma_s} \rho_0 \eta g v \, d\sigma + c_f^2 \int_{\Gamma_s} \dot{\varphi} v d\sigma - c_f^2 U \int_{\Gamma_s} \nabla_s \varphi_0 \cdot \nabla_s v \varphi + v \Delta_s \varphi_0 \varphi d\sigma \\
&+ \left[c_f^2 U \frac{\partial \varphi_0}{\partial \nu_s} \varphi v + 2\varepsilon c_f^2 c_r \dot{\eta} v \right]_{\partial \Gamma_s} = 0.
\end{aligned} \tag{19}$$

Physical field approximation is performed by classical finite element method. A finite dimension subspace $V_h \subset H^1(\overline{\Omega})$ made of piecewice linear functions on a fixed mesh, characterized by element length h, is considered. Letting $V_h = span(\varphi_1, \varphi_2, \ldots, \varphi_{N1}, \eta_1, \eta_2, \ldots, \eta_{N2})$ with $\varphi_{i\ 1 \le i \le N1}$ and $\eta_{i\ 1 \le i \le N2}$ finite element shape functions on Ω and on Γ_s respectively. Calling X the coordinate vector of $\mathscr{X}(\varphi, \eta)$ relative to this basis leads to the recasted algebraic differential linear problem :

Find $X(t) \in R^N$, $N = N1 + N2$, $t \in]0, T[$ such that

$$M\ddot{X} + C\dot{X} + KX = 0 \tag{20}$$

with $X(0), \dot{X}(0)$ prescribed. M, C, K are sparses matrices. Centered finite difference schemes are applied for the time domain approximation in order to avoid numerical instabilities. Finally the problem becomes :

Find $X^{(n)} \in R^N$, $n > 1$, such that

$$A_1 X^{(n+1)} = A_2 X^{(n)} + A_3 X^{(n-1)} \tag{21}$$

where A_1, A_2 et A_3 are sparse matrices depending on M, C, K and Δt with Δt the time step chosen.

The computing process is fully automated. All the geometry operations and meshes are generated and updated automatically according intermediate results by a batch program using Numpy and Scipy Python routines and GMSH [25]. Due to the complexity of weak formulation terms, low-level generic assembly procedures of GETFEM++ is employed to make the assembly of the involved sparse matrices in Eq.(20) [26]. To compute the solution of the large sparse system Eq.(21) a MUMPS solver is used. For the post processing handling, Matplotlib python libraries, PARAVIEW and GMSH are utilized [27]. Mesh convergence study is performed by reducing characteristic size of elements, h, from $h = 10^{-3}$ to $h = 6.25 \times 10^{-5}$. As shown in figures 4 and 5, results converge upon a solution as the mesh density increases. A satisfactory compromise between accuracy of results and computing time can be achieved by choosing the value of $h = 1.25 \times 10^{-4}$. For numerical computations, values of parameters of table 4.1 are used.

Parameters	L(m)	H(m)	R(m)	U(m.s^{-1})	ε (m)	σ (N.m^{-1})
Values	1	1	5.10^{-2}	0.15	10^{-3}	0.075

Table 1. Numerical computational values of parameters of the problem

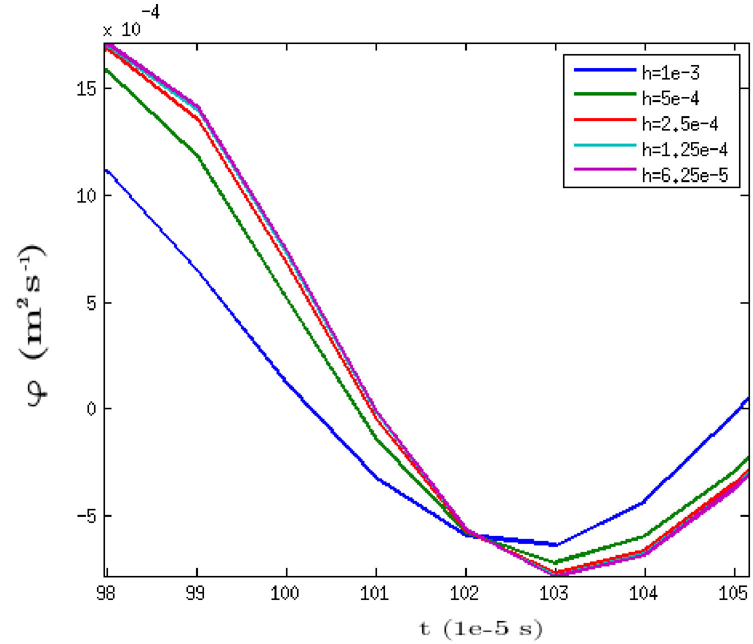

Figure 4. Inner fluid velocity potential $\varphi\,(\mathrm{m}^2 s^{-1})$ at point of coordinates $(0.5, 0.5)$ versus time $(10^{-5} s)$ for different elements sizes of the mesh.

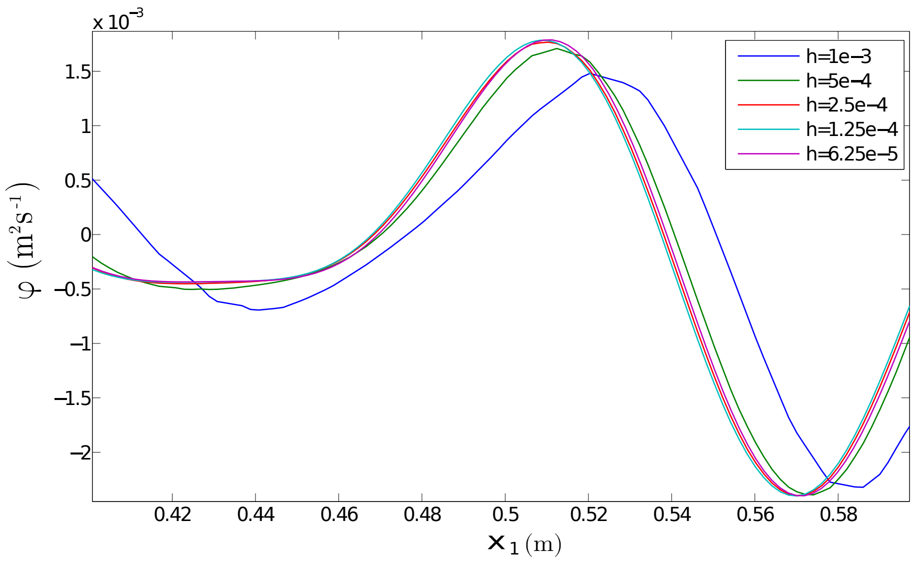

Figure 5. Inner fluid velocity potential $\varphi\,(\mathrm{m}^2 s^{-1})$ for different mesh densities along a part of the middle line of computational domain (m) at $t = 100\Delta t_v$.

5. Results and comments

Wave propagation phenomenon is monitored by the variation of φ in the inner fluid and the variation of η on the surface respectively. The value of time step chosen is $\Delta t_v = 10^{-5} s$ in order to see properly wave propagation with a velocity of c_f across the extend of the computational domain Ω. As it can be seen on figure 6, reflecting waves appear on the bottom of the domain as on the surface of the immersed solid body where homogeneous Neumann conditions are imposed to model non penetrability of the fluid through them. In addition, on both lateral sides of the computational domain no spurious reflecting wave appears to be present. Thanks to hyperbolicity of the problem, in order to verify whether non-reflecting boundary conditions are satisfactory on inner fluid lateral edges Eq.(16), a similar study is carried out according to the same previous calculation criteria on a larger computational domain in x_1 direction, sized so as to avoid lateral side spurious reflecting waves during the all simulation time [17]. The new solution obtained is regarded as a reference solution. Both resulting waves are in phase but a variable amplitude difference can be noticed. The wave is slightly reflected especially on its peak of amplitude for times when there are not many interference. Indeed absorbing boundary conditions chosen are not intended to handle such a situation (see figure 7).

Waves propagation in inner fluid results in deformation of the surface as shown in figures 8 and 9. The corresponding normal displacement η propagates along the surface Γ_s. On each side of the surface, $\partial\Gamma_s$, no spurious reflective wave is noticed. In inner fluid layer no wave related with any reflective surface on surface is neither observed (see figure 9). Then lateral boundary conditions introduced by Eq.(17) seem to be also adequate to successfully model the propagating phenomenon on the surface. Nevertheless the velocity of the phenomenon is the same as in inner fluid layer which is not in complete agreement with surface layer material properties and wave propagation in stratified media theories [1,11]. The expected value should be closed to the riddle velocity c_r. Therefore no surface propagation phenomenon should be observed with time step Δt_v. That's actually what happens when initial disturbance is located just below or on the surface as shown in figure 10. The observed normal displacements η in figures 8 and 9 are not related directly to surface wave propagation, but rather primarily to the potential volume wave propagation in inner fluid layer and to the interface coupling between the potential φ and the normal displacement η on Γ_s given by Eq.(14). The energy transmitted to the surface layer by the inner layer remains stationary over the time range considered. Therefore application of lateral boundary conditions Eq.(17) does not significantly affect the propagation phenomenon and its accuracy can not be estimated with an initial perturbation in inner fluid layer.

Numerical simulations are then carried out in the case of an initial disturbance of the surface with a time step $\Delta t_s = 10^{-2} s$. The functions $\varphi(x,0)$ and $\partial\varphi/\partial t(x,0)$ are set to zero in Ω and $\eta(x,0)$ and $\partial\eta/\partial t(x,0)$ are introduced as Gaussian pulse functions on Γ_s. Surface waves propagate along Γ_s (see figures 10 and 11) but singularities appear on each side of the surface $\partial\Gamma_s$ as shown on figure 12. In fact due to the significant difference between the wave propagation characteristic velocity values of the surface and inner fluid layers, singularities come out on the intersection between the artificially chosen boundaries of the domain and the two layers' interface when Sommerfeld non reflecting boundary conditions are applied [28]. The non reflecting boundary condition on the lateral edges Eq.(13) has to be changed to handle these difficulties [29]. To this end, as the conditions are to be set for the points $\partial\Gamma_s$ that belong to the surface Γ_s and to the lateral boundaries Γ_{1equi} or Γ_{2equi}, the equations Eq.(13), Eq.(14) and Eq.(16) are considered to devise the new boundary conditions. The guiding idea is to extend the non reflective boundary condition applied on the lateral boundaries Γ_{1equi} or Γ_{2equi} Eq.(16) to the surface Γ_s intersecting

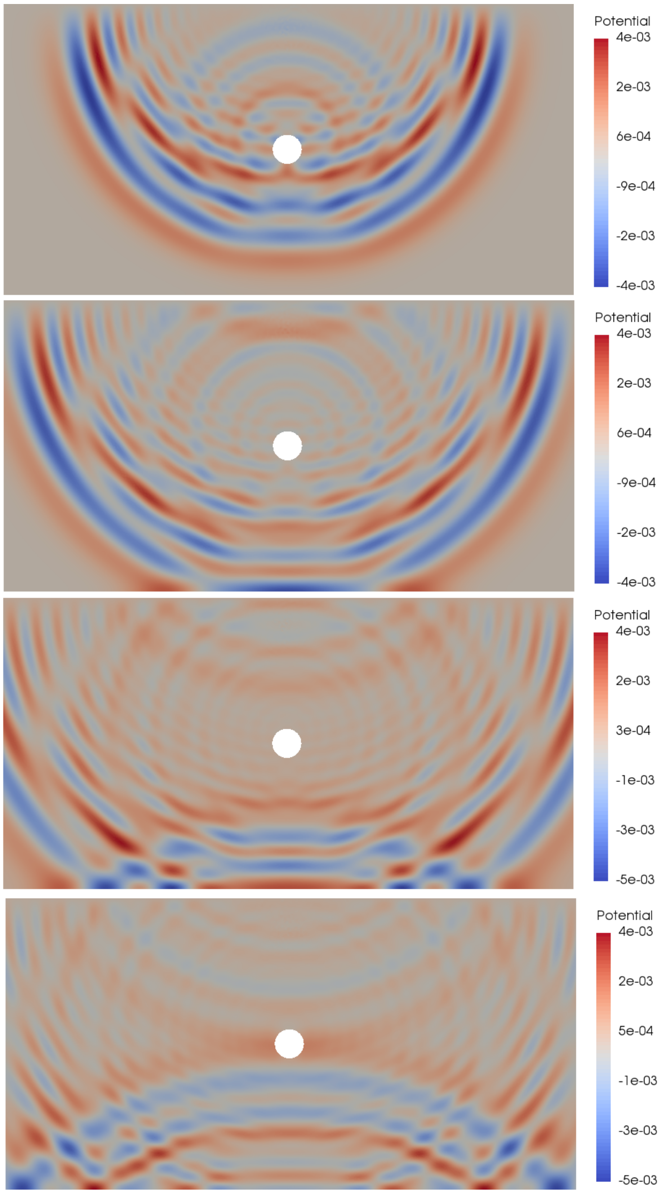

Figure 6. Propagation of velocity potential disturbance φ at times: $t = 80\Delta t_v$, $t = 100\Delta t_v$, $t = 120\Delta t_v$, $t = 140\Delta t_v$. The order of magnitude of initial perturbation is $10^{-2}\mathrm{m}^2 s^{-1}$.

points $\partial\Gamma_s$ Eq.(13) by means of the normal velocity continuity condition Eq.(14). Using the simplifying assumptions $\varphi_0 = x_1$, $s = x_1$ and $(v_s.e_1) = \pm 1$ led by choosing Γ_{1equi} and Γ_{2equi} away from rigid body, the following simplified equations must be satisfied on $\partial\Gamma_s$:

$$\frac{\partial^2\eta}{\partial t^2} + 2U\frac{\partial^2\eta}{\partial x_1 \partial t} + \left(U^2 - c_r^2\right)\frac{\partial^2\eta}{\partial x_1^2} + \frac{1}{2\varepsilon}\left(\frac{\partial\varphi}{\partial t} + \mathrm{U}\frac{\partial\varphi}{\partial x_1}\right) + \frac{g}{2\varepsilon}\eta = 0, \tag{22}$$

$$\frac{\partial\varphi}{\partial x_2} = \frac{\partial\eta}{\partial t} + U\frac{\partial\eta}{\partial x_1}, \tag{23}$$

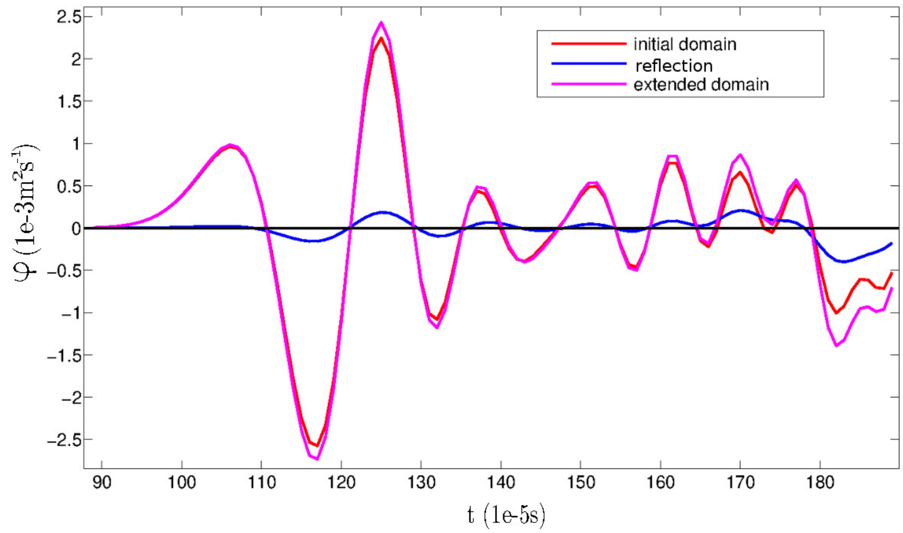

Figure 7. Comparison of inner fluid velocity potentials φ ($10^{-3}\mathrm{m}^2 s^{-1}$) versus time ($10^{-5} s$) between extended and main computational domain on the middle of right artificial lateral edge.

$$\frac{\partial \varphi}{\partial t} + \left(U + c_f\right) \frac{\partial \varphi}{\partial x_1} = 0 \quad \text{on} \quad \Gamma_s \cap \Gamma_{2equi}, \tag{24}$$

$$\frac{\partial \varphi}{\partial t} + \left(U - c_f\right) \frac{\partial \varphi}{\partial x_1} = 0 \quad \text{on} \quad \Gamma_s \cap \Gamma_{1equi}. \tag{25}$$

For the right side (resp. the left side), the solution method consists in derivating first Eq.(24) (resp. Eq.(25)) with respect to x_2 and Eq.(23) with respect to x_1 and t, in order to eliminate partial derivatives of φ. Introducing the resulting expression into Eq.(22) leads, after integrating with respect to time, to the following new boundary condition in cartesian coordinates for each edge,

$$Z^{\pm} \frac{\partial \eta}{\partial t} + A^{\pm} \frac{\partial \eta}{\partial x_1} + B^{\pm} \int_0^t \eta \, ds + C^{\pm} \varphi = 0 \quad \text{on} \quad \partial \Gamma_s^{\pm} \tag{26}$$

with $A^{\pm}, B^{\pm}, C^{\pm}, Z^{\pm}$ depending on U, c_f, c_r, ϵ, g. The symbol $^-$ denotes that condition is on the left boundary of Γ_s and $^+$ on the right one. The boundary conditions obtained are said non local in time as they depend not only on the time t but also on entire history of η on $\partial\Gamma_s$. The second part of variational formulation Eq.(19) becomes within the new non reflective boundary conditions Eq.(26):

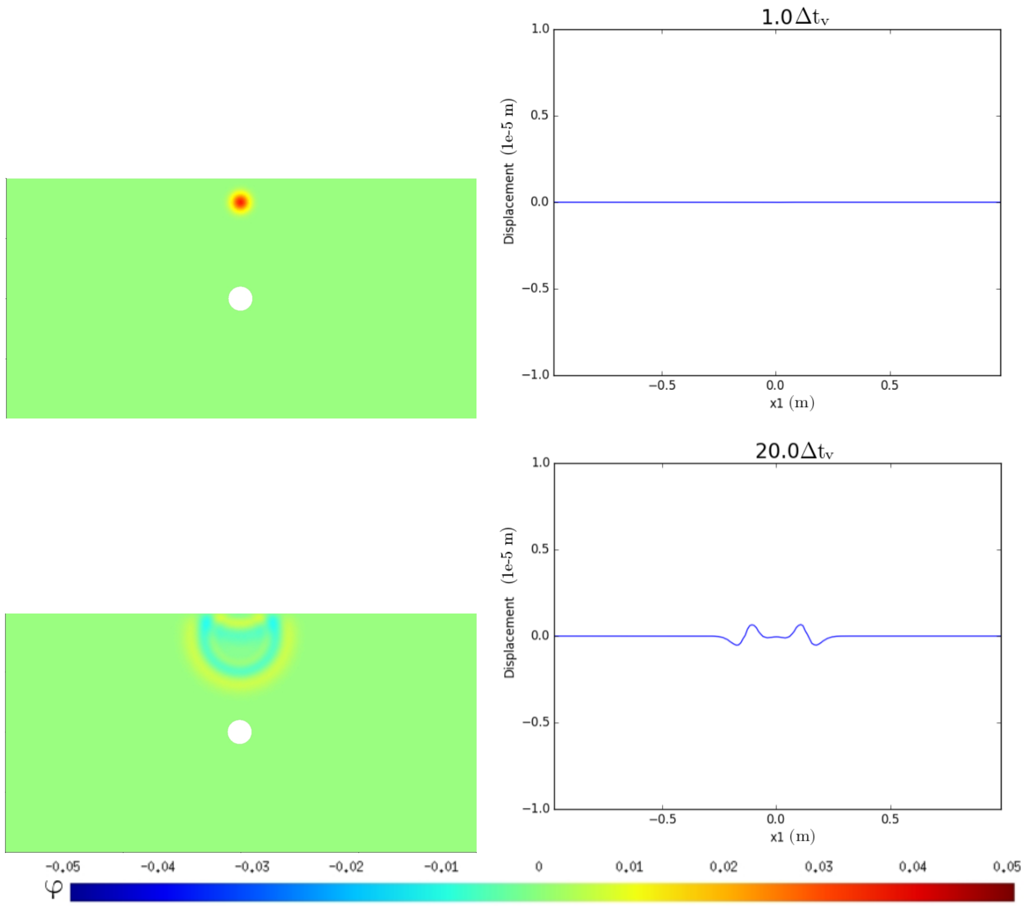

Figure 8. Propagation of disturbance φ in Ω and related normal surface displacement η (10^{-5}m) on Γ_s versus x_1 coordinate (m) at times: $t = \Delta t_v$, $t = 20\Delta t_v$. The initial order of magnitude of φ is $10^{-2}\mathrm{m}^2 s^{-1}$. Its propagating order of magnitude is $10^{-3}\mathrm{m}^2 s^{-1}$ and the order of magnitude of the normal displacement is 10^{-6}m.

$$
\begin{aligned}
&2\varepsilon {c_f}^2 \int_{\Gamma_s} \left(\ddot{\eta} v + U \nabla_s \varphi_0 \left(\nabla_s \dot{\eta} v - \dot{\eta} \nabla_s v\right) - U^2 (\nabla_s \varphi_0 \cdot \nabla_s \eta)(\nabla_s \varphi_0 \cdot \nabla_s v)\right) d\sigma \\
&-2\varepsilon {c_f}^2 U \int_{\Gamma_s} \left(U v \Delta_s \varphi_0 \left(\nabla_s \varphi_0 \cdot \nabla_s \eta\right) + v \Delta_s \varphi_0 \dot{\eta}\right) d\sigma + \frac{c_f^2}{\rho_0} \int_{\Gamma_s} \sigma \nabla_s \eta . \nabla_s v \, d\sigma \\
&+ \frac{c_f^2}{\rho_0} \int_{\Gamma_s} \rho_0 \eta g v \, d\sigma + c_f^2 \int_{\Gamma_s} \dot{\varphi} v d\sigma - c_f^2 U \int_{\Gamma_s} \nabla_s \varphi_0 \cdot \nabla_s v \varphi + v \Delta_s \varphi_0 \varphi d\sigma \\
&+ \left[\left(E^{\pm} \dot{\eta} + F^{\pm} \int_0^t \eta \, ds + G^{\pm} \varphi \right) v \right]_{\partial \Gamma_s} = 0.
\end{aligned}
\tag{27}
$$

with $E^{\pm}, F^{\pm}, G^{\pm}$ depending on U, c_f, c_r, ϵ, g. The previous solution method is used to solve the new variationnal problem Eq.(18) and Eq.(27). For the time domain approximation, centered

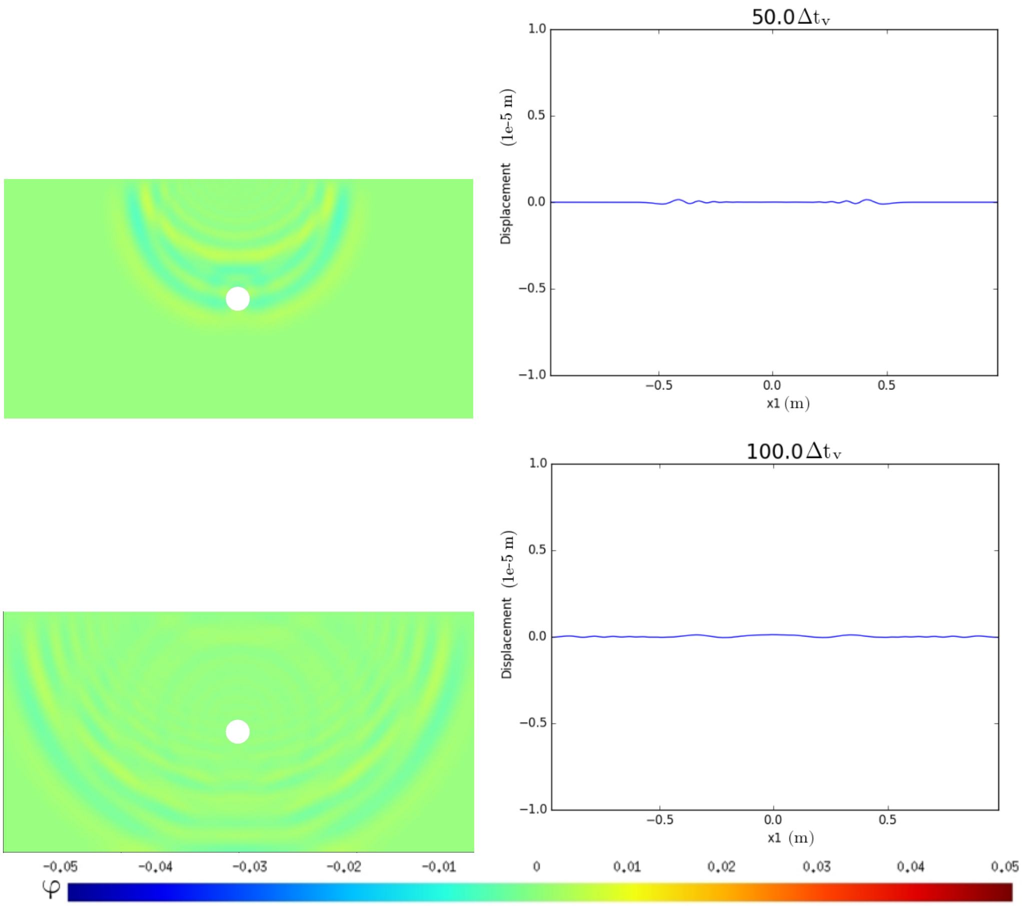

Figure 9. Propagation of disturbance φ in Ω and related normal surface displacement $\eta\,(10^{-5}\mathrm{m})$ on Γ_s versus $x_1(m)$ coordinate at times: $t = 50\Delta t_v$, $t = 100\Delta t_v$. Its order of magnitude is $10^{-3}\mathrm{m}^2 s^{-1}$ and corresponding normal displacement η order of magnitude is 10^{-6}m.

finite difference scheme is applied for derivatives and trapezoidal rule is used for the integral over time term. The problem becomes finding $X^{(n)} \in R^N$, $n > 1$, such that

$$A_1 X^{(n+1)} = A_2 X^{(n)} + A_3 X^{(n-1)} + F \tag{28}$$

where A_1, A_2 et A_3 are sparse matrices depending on M, C, K and Δt ; F a vector depending on $F^{\pm}$ and Δt accounting for non local condition term in time Eq.(26) with non zero component corresponding to the surface edges $\partial\Gamma_s$.

A numerical simulation is carried out with an initial surface excitation and a time step Δt_s. Singularities seem to be no longer present on $\partial\Gamma_s$ and waves can get out of computational domain without generating significant spurious reflections (see figure 13). Comparison between the old and the new non reflective boundary condition results is done over two thousand time steps Δt_s to check any singularities (see figure 15). Similarly to the previous case to verify non-reflecting boundary conditions on surface edges Eq.(26), a larger computational domain in x_1 direction

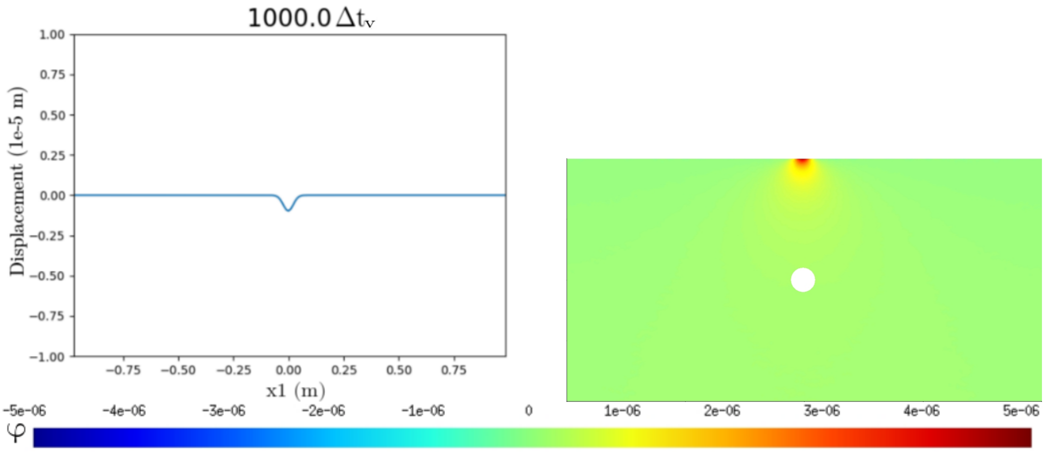

Figure 10. Propagation of normal surface displacement η on Γ_s versus x_1 coordinate and related disturbance φ in Ω at time $t = 1000\Delta t_v = \Delta t_s$. Initial perturbation is located on the surface of the fluid. The order of magnitude of η is 10^{-6}m. The order of magnitude of the potential φ transmitted to the surface of inner fluid is $10^{-6}\text{m}^2 s^{-1}$.

is chosen to compute a reference solution. Both resulting waves are in phase but a varying amplitude difference can be noticed due to existing spurious reflections (see figure 14) which fade away over time (see figure 13). According to the ratio between the orders of magnitude of the inner fluid potential and the surface displacement noticed in each calculated cases, it comes out that the inner fluid wave propagation effect is not significant in the case of initial disturbance nearby the surface or on the surface itself. Indeed, a velocity potential of order of magnitude of $10^{-3}\text{m}^2 s^{-1}$ on the surface leads to a normal displacement response of order of magnitude of 10^{-6}m in inner fluid initial perturbation case. But in surface initial disturbance case where the order of magnitude of normal displacement is 10^{-6}m, the velocity potential barely reaches $10^{-6}\text{m}^2 s^{-1}$ on the surface, the linearity of the model leads to a normal displacement response of 10^{-9}m, therefore negligible compared to 10^{-6}m (see figures 8, 9, 10 and 11). Thus the waves propagate mainly in the surface layer guided in the medium of smaller velocity in totally agreement with wave propagation theories in stratified media. Actually, during surface wave propagation, a small amount of energy is steadily transferred from the surface to inner fluid which is immediately removed from the computational domain as in an incompressible fluid. The velocity potential φ rendering (see figure 11) comes from the superposition of all velocity potential waves generated by the propagating surface wave at all times. Therefore these results can hardly be analyzed and used to clearly draw any possible conclusions on the compliance of the non reflecting boundary condition chosen Eq.(16) in inner fluid layer.

6. Conclusion

For the modelling of the wake of a solid body moving through a body of water, a wave propagation problem in a convective stratified media is considered. In order to apply standard methods of resolution intended for bounded domains, artificial boundaries are introduced and appropriate non-reflecting boundary conditions are sought. Since the significant differences between layer properties make difficult to address the entire problem with traditional approximations, a non local in time boundary condition has been devised by taking into account all the conditions that

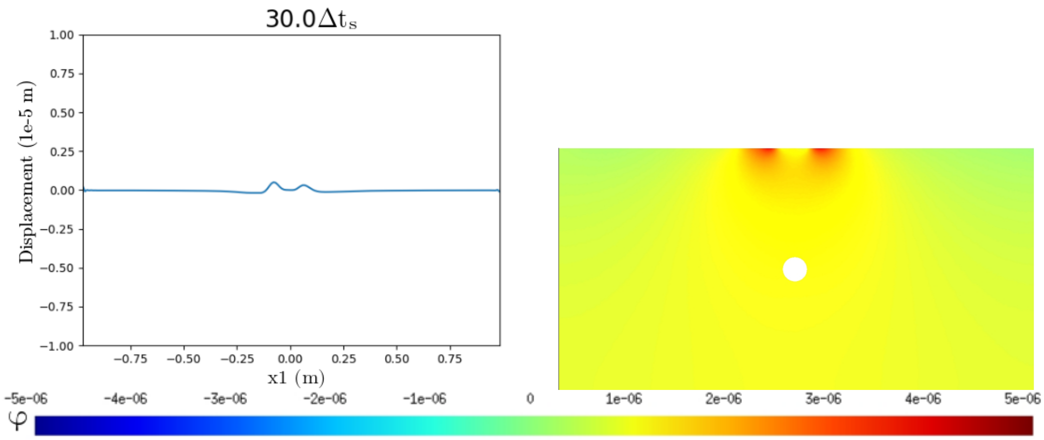

Figure 11. Propagation of normal surface displacement η on Γ_s versus x_1 coordinate and related disturbance φ in Ω at time $t = 30\Delta t_s$. Initial disturbance is located on the surface of the fluid. Order of magnitude of propagating η is 10^{-6}m. The order of magnitude of the potential φ transmitted to the surface of inner fluid is $10^{-6}\text{m}^2 s^{-1}$.

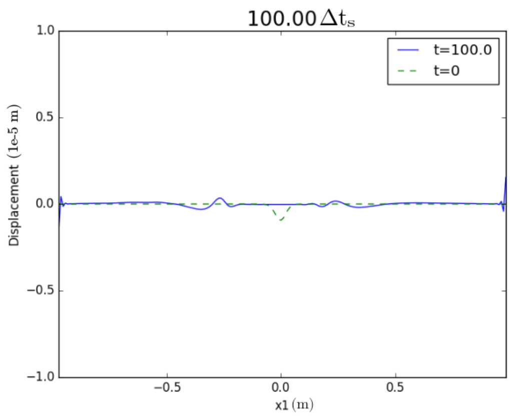

Figure 12. Displacement $\eta\,(10^{-5}m)$ of the surface Γ_s at time $t = 100\Delta t_s$ versus x_1 coordinate (m). Initial disturbance is located on the surface Γ_s in dash point. Sigularities appear on the edges of the surface $\partial\Gamma_s$.

must be met on the artificial lateral edges of the computational domain. This work highlighted a complex phenomenon which involves coupled surface and bulk waves propagations at different time scales and with very different orders of magnitude. These features cannot be observed in the assumption of incompressibility of the fluid made in common studies. Further works have to be carried out on non reflecting boundary condition to fully eliminate the reflections of the wave in line with reference results without complicating the formulation of the problem or increasing the amount of calculation.

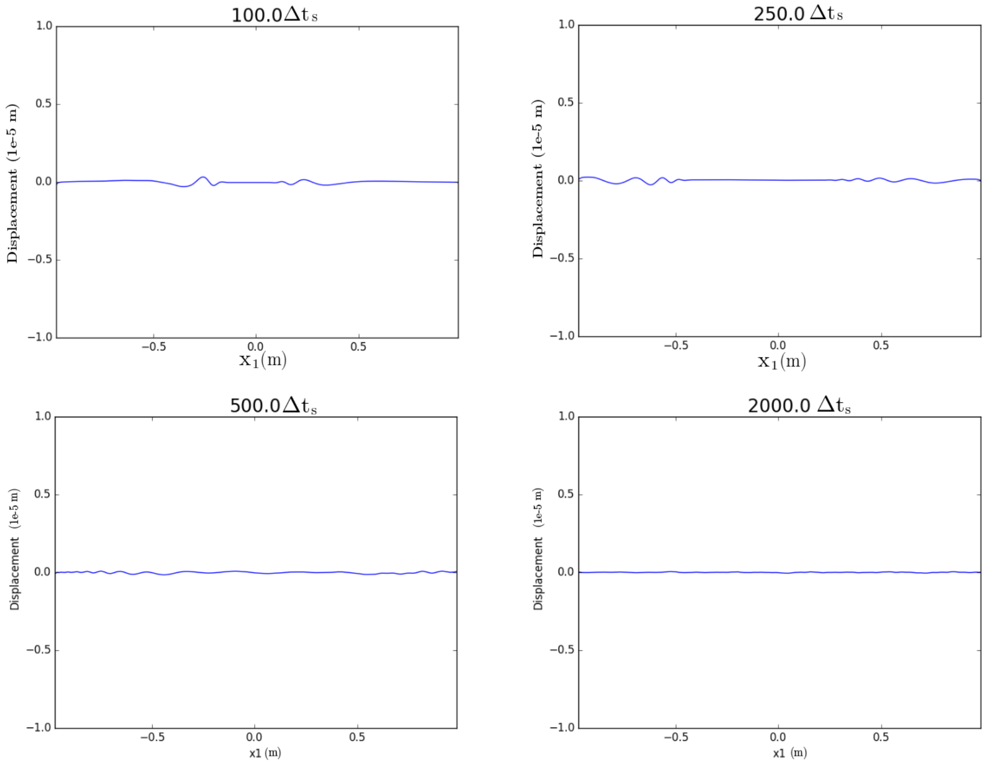

Figure 13. Displacement $\eta(10^{-5}m)$ of the surface Γ_s versus x_1 coordinate (m) at: $t = 100\Delta t_s$, $t = 250\Delta t_s$, $t = 500\Delta t_s$ and $t = 2000\Delta t_s$. Initial disturbance is located on the surface Γ_s. The waves propagate without any singularity on surface edges but spurious reflections on surface are still present

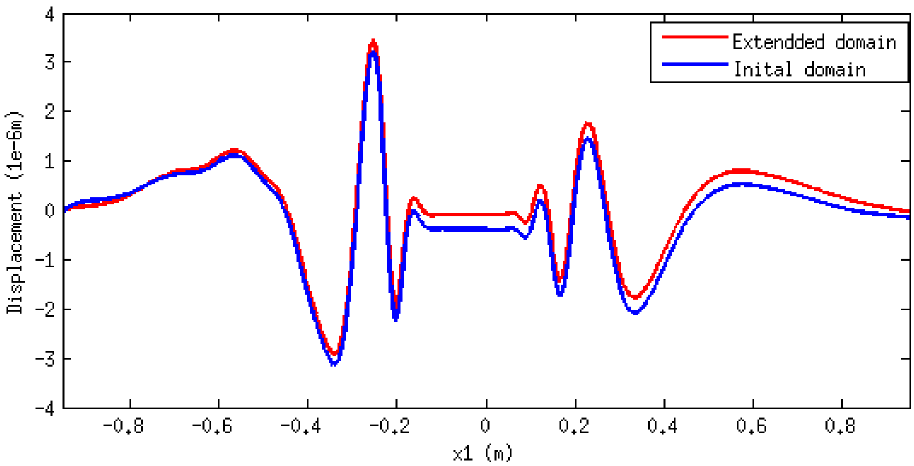

Figure 14. Comparison between normal displacements $\eta(10^{-6}m)$ of surface Γ_s in initial and extended domain cases versus $x_1(m)$ at $t = 100\Delta t_s$.

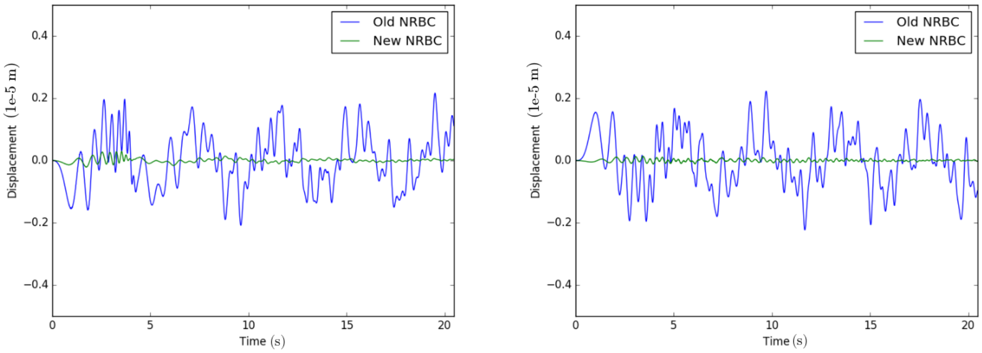

Figure 15. Comparison of the results for displacement $\eta(10^{-5}m)$ at $\partial\Gamma_s^-$ and at $\partial\Gamma^+$ obtained by the two non reflective boundary conditions (NRBC) and over simulation time $2000\Delta t_s$.

Acknowledgment

I would like to thank Professor Philippe Destuynder, at University of La Rochelle (Laboratory LaSIE), for fruitful discussions.

References

[1] L. Brekhovskikh, *Waves in layered media*, vol. 16, Elsevier, 2012.

[2] F. Dias, A. Dyachenko, V. Zakharov, "Theory of weakly damped free-surface flows: A new formulation based on potential flow solutions", *Physics Letters A* **372** (2008), no. 8, p. 1297 - 1302.

[3] J. Lighthill, *Waves in fluids*, Cambridge university press, 2001.

[4] M. S. Longuet-Higgins, "Eulerian and Lagrangian aspects of surface waves", *Journal of Fluid Mechanics* **173** (1986), p. 683–707.

[5] J. W. Miles, "On the generation of surface waves by shear flows", *Journal of Fluid Mechanics* **3** (1957), no. 02, p. 185-204.

[6] J. Stocker, "Water waves", *Pure and Applied Mathematics* **9** (1957), p. 291-314.

[7] M. Bauer, "Le problème de Neumann-Kelvin", *Annali di Matematica Pura ed Applicata* **124** (1980), no. 1, p. 233-255.

[8] A. Cariou, "Une méthode de calcul par éléments finis de la résistence de vague des corps flottants ou immergés en théorie linéaire", *Revue de l'Institut Français du Pétrole* **33** (1978), no. 1, p. 59-82.

[9] P. Guével, G. Delhommeau, D. Euvrard, S. Marcouyoux, "Résistance d'ondes d'un navire de surface", *La Houille Blanche* **1977** (1977), no. 5-6, p. 429-439.

[10] R. L. Higdon, "Absorbing boundary conditions for acoustic and elastic waves in stratified media", *Journal of Computational Physics* **101** (1992), no. 2, p. 386-418.

[11] A. H. Nayfeh, *Wave propagation in layered anisotropic media: With application to composites*, Elsevier, 1995.

[12] H. Hellsten, V. Maz'ya, B. Vainberg, "The spectrum of water waves produced by moving point sources, and a related inverse problem", *Wave motion* **38** (2003), no. 4, p. 345-354.

[13] O. V. Motygin, "On the statement of the three-dimensional Neumann-Kelvin problem", in *2008 Proceedings of the International Conference Days on Diffraction*, June 2008, p. 140-146.

[14] P. Destuynder, C. Fabre, "A discussion on Neumann–Kelvin's model for progressive water waves", *Applicable Analysis* **90** (2011), no. 12, p. 1851-1876.

[15] B. Engquist, A. Majda, "Absorbing boundary conditions for numerical simulation of waves", *Proceedings of the National Academy of Sciences* **74** (1977), no. 5, p. 1765-1766.

[16] L. Halpern, "Absorbing boundary conditions for the discretization schemes of the one-dimensional wave equation", *Mathematics of Computation* **38** (1982), no. 158, p. 415-429.

[17] E. Bécache, D. Givoli, T. Hagstrom, "High-order absorbing boundary conditions for anisotropic and convective wave equations", *Journal of Computational Physics* **229** (2010), no. 4, p. 1099-1129.

[18] E. Bécache, A. B.-B. Dhia, G. Legendre, "Perfectly matched layers for the convected Helmholtz equation", *SIAM Journal on Numerical Analysis* **42** (2004), no. 1, p. 409-433.

[19] J.-P. Berenger, "A perfectly matched layer for the absorption of electromagnetic waves", *Journal of computational physics* **114** (1994), no. 2, p. 185-200.

[20] A. Bermúdez, L. Hervella-Nieto, A. Prieto, R. Rodrí *et al.*, "An optimal perfectly matched layer with unbounded absorbing function for time-harmonic acoustic scattering problems", *Journal of Computational Physics* **223** (2007), no. 2, p. 469-488.

[21] T. Hagstrom, "Radiation boundary conditions for the numerical simulation of waves", *Acta numerica* **8** (1999), p. 47-106.

[22] R. L. Higdon, "Absorbing boundary conditions for acoustic and elastic waves in stratified media", *Journal of Computational Physics* **101** (1992), no. 2, p. 386-418.

[23] D. Givoli, *Numerical methods for problems in infinite domains*, vol. 33, Elsevier, 2013.

[24] P. Destuynder, C. Fabre, "Modélisation du comportement hydrodynamique des bateaux", Lecture, Jun 2012.

[25] C. Geuzaine, J.-F. Remacle, "Gmsh: A 3-D finite element mesh generator with built-in pre-and post-processing facilities", *International journal for numerical methods in engineering* **79** (2009), no. 11, p. 1309-1331.

[26] Y. Renard, K. Poulios, "GetFEM: Automated FE modeling of multiphysics problems based on a generic weak form language", *ACM Transactions on Mathematical Software (TOMS)* **47** (2020), no. 1, p. 1-31.

[27] J. Ahrens, B. Geveci, C. Law, "Paraview: An end-user tool for large data visualization", *The visualization handbook* **717** (2005), no. 8.

[28] P. Destuynder, C. Fabre, "Singularities occurring in multimaterials with transparent boundary conditions", *Quarterly of Applied Mathematics* **74** (2016), no. 3, p. 443-463.

[29] M. López de Silanes *et al.*, *Fourteenth International Conference Zaragoza–Pau on Mathematics and its Applications: Jaca (Spain), September 12*, vol. 41, Prensas de la Universidad de Zaragoza, 2018, 149-158 pages.